Bioconvection Maxwell nanofluid flow over a stretching cylinder influenced by chemically reactive activation energy surrounded by a permeable medium

Arshad Khan[1]*, Zahoor Iqbal[2,3], N. Ameer Ahammad[4],
Maawiya Ould Sidi[5], Samia Elattar[6], Somia Awad[7], El Sayed Yousef[8,9]
and Sayed M Eldin[10]

[1]College of Aeronautical Engineering, National University of Sciences and Technology (NUST), Islamabad,
Pakistan, [2]Department of Mathematics, Quaid-i-Azam University, Islamabad, Pakistan, [3]Shenzhen Institutes
of Advanced Technology, Chinese Academy of Sciences, Shenzhen, China, [4]Department of Mathematics,
Faculty of Science, University of Tabuk, Tabuk, Saudi Arabia, [5]RT-M2A Laboratory, Mathematics Department,
College of Science, Jouf University, Sakaka, Saudi Arabia, [6]Department of Industrial and Systems Engineering,
College of Engineering, Princess Nourah bint Abdulrahman University, Riyadh, Saudi Arabia, [7]Physics
Department, Al-Qunfudah University College, Umm Al-Qura university, Mecca, Saudi Arabia, [8]Physics Dep,
Faculty of Science, King Khalid University, Abha, Saudi Arabia, [9]Research Center for Advanced Materials
Science (RCAMS), King Khalid University, Abha, Saudi Arabia, [10]Center of Research, Faculty of Engineering,
Future University in Egypt, New Cairo, Egypt

The role of nanofluids in the development of many electronic devices at the industrial level is very significant. This investigation describes the thermal exploration for a bioconvective flow of Maxwell nanoparticles over stretching and revolving the cylinder placed in a porous medium. The fluid flow is in contact with chemically reactive activation energy. The swirling flow is induced by the stretching rotary cylinder. The magnetic effect of constant strength B_0 is practiced to the flow system in combination with thermally radiative effects and a heat source/sink for controlling the thermal effects upon the flow system. The thermophoretic and Brownian motion characteristics, due to the nanofluid flow, are captured by implementing the Buongiorno model. The central focus of this study is to explore the thermal and mass transfer for the flow problem accompanied by motile microorganisms. The governing equations have been converted to the dimensionless form with similar variables, and the homotopy analysis method (HAM) has then been applied for solution. It has been concluded in this investigation that fluid flow decays for escalation in the Maxwell, porosity, and magnetic parameters, and Forchheimer and bioconvection Rayleigh numbers, while upsurges with the augmenting values of the Buoyancy factor. With the increasing values of the Brownian number, thermophoretic and radiation factors upsurge the thermal profiles and decline the concentration profiles. Moreover, the density of motile microorganisms declines with the expansion in the Peclet number. The range for η is taken from 0 to seven to get the convergence of the graph.

KEYWORDS

Maxwell nanofluid, stretching cylinder, bioconvection flow, porous medium, Arrhenius activation energy, HAM

Introduction

Bioconvection is the scattering of gyrotactic microorganisms through a contracted deferment. It is the convective fluid flow at the microscopic level due to the variations in density, which is produced by the collective spinning of motile microorganisms. The spinning characteristics of gyrotactic microorganisms are of dynamic significance to comprehend a number of biological characteristics associated with bioconvection. This awareness of bioconvection was first introduced by Platt [1] for investigating its pattern through free swimming in a dense culture. Ahmad et al. [2] inspected the bioconvective Maxwell nanofluid flow with thermally radiative effects. Sajid et al [3] studied the influence of microorganisms along with variable diffusivity of species for blood-gold Reiner–Philippoff nanoparticles. Waqas et al. [4] numerically simulated the bioconvective nanofluid flow with the influence of motile microorganisms and have numerically revealed the impact of different factors upon flow profiles. Shahzad et al. [5] explored the electro magnetohydrodynamics (EMHD) nanoliquid flow past an extending sheet with the influence of microorganisms and have concluded that thermal flow has augmented with the growth in the thermal Biot number. Safdar et al. [6] discussed the EMHD nanofluid flow past an extending sheet subjected to microorganisms and effects of Arrhenius activation energy and have claimed that thermal profiles have augmented with growth in the values of the mixed convective factor. Abdelmalek et al. [7] mathematically established a model for the bioconvective flow of nanoliquids past a revolving cylinder. The slip effects along with thermal conductivity have been used to the flow system by the authors of this study and then have been used to determine the approximate solution of the resultant equations. Hamid et al. [8] numerically studied the bioconvective magnetohydrodynamics (MHD) nanofluid flow with the influence of microorganisms and have revealed that thermal distribution has augmented with an upsurge in the Biot number and radiation factor. Rana et al. [9] scrutinized the swimming process of microbes in blood flow with the nano-bioconvection Williamson fluid model. In this study, the finite difference method has been used by the authors to carry out the stability and convergence analysis.

The transfer of mass in different species normally takes place for variations related to such species. The migration of species in such a phenomenon from a region of higher to lower concentration has been observed. Examples include handling of foods, diffusion of nutrients, and thermal insulation. In the past few decades, mass transfer using chemical reactions has persisted in an interested area for various researchers. Chamkha et al. [10] studied the mass and thermal flows for varying thermal and mass diffusions with the influence of chemical reactions and have revealed that fluid motion has declined with growth in the chemical factor, due to which less mass has diffused. Mabood et al. [11] explored the micropolar fluid flow upon a thin moving needle subjected to Soret and Dufour effects and have established that the micropolar factor has upsurged the rotary motion. Sarada et al. [12] studied the influence of exponentially growing inner heat generation over the trihybrid nanoliquid flow over an extending curved sheet. The lowest essential energy for starting a reaction chemically is called the activation energy. This term was first familiarized by Arrhenius [13]. The activation energy is the magnitude of energy that is mandatory for a reactant to convert into a product. It is understood that all molecules have some energy either in the form of potential energy or kinetic energy. This energy can be used to first stretch, then to turn, and finally to disrupt the bonds among the molecules that lead to a chemical reaction. The idea of activation energy is closely related to oil emulsion and oil repository engineering. In recent
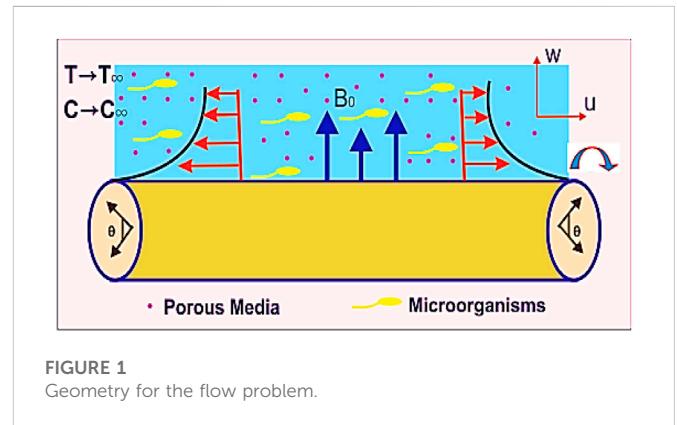
FIGURE 1
Geometry for the flow problem.

times, the collective impact of chemically reactive activation energy has gained more importance due to its applications in industries. Many investigations have been carried out with the main focus upon the concept of mass transfer in a flow system. Maleque [14] investigated the impact of activation energy upon the MHD flow past a penetrable medium. Jayaparkash et al. [15] studied the activation energy and heat convection for the radiative hybrid nanofluid flow over a curved surface. Sajid et al. [16] elaborated the influences of chemically reactive energy of the trihybrid nanoparticle flow over the wedge and have concluded that the heat flow behavior of the fluid has amplified for three nanoparticle suspensions in pure fluids.

The mixing of nano-sized particles in the base fluid is termed as the nanofluid. It has revealed that the heat conduction characteristics of the pure fluid augment by combining the nanoparticles to pure fluids. Since the nanofluid has augmented heat convection characteristics, these fluids have numerous engineering and industrial applications, like solar collectors and radiators, and hybrid power engines. Different established works can be found with the main focus upon the heat transfer characteristics by applying different flow conditions and geometries. Choi [17] stood as the first nobleman to propose the use of nanoparticles in pure fluids. Sajid et al. [18–20] deliberated upon fluid flow and heat transfer using different physical flow geometries and various flow conditions subjected to suspension of nanoparticles in pure fluids. Saleem et al. [21] deliberated the water-based nanofluid flow past a horizontal sheet using three different shapes of nanoparticles. Cao et al. [22] simulated the dynamical colloidal combination of nanoparticles and water using different levels of slips of partial nature. Animasaun et al. [23] deliberated on trihybrid nanoparticle flow over a heated surface and have concluded that heat flow has been augmented with the growth in volume fraction. Xiu et al. [24] examined the nanofluid flow for a dual-stretched wage surface using forced convective effects subjected to variations in temperature.

The flow of fluids upon stretching cylinders has appealed the intuition of various scientists and researchers. Its different applications include crystal production, paper manufacturing, fabrication of glass, and polymer extrusion. Due to such important applications of flow over stretching cylinders, many investigations have been carried out for these flows with the main emphasis upon thermal and mass transfer. Kumar et al. [25] studied the MHD hybrid nanofluid flow past a stretching cylinder and have concluded that fluid motion has declined with the upsurge in the ferromagnetic factor. Naveen Kumar et al. [26] conducted a detailed study on the ferromagnetic fluid flow upon a stretching cylinder. Varun Kumar et al. [27] used the modified Fourier thermal flux for investigating

TABLE 1 Depiction of substantial parameters.

Notation	Mathematical value	Physical depiction
N_b	$\tau D_B \Delta C / v$	Brownian motion parameter
M	$\sigma B_0{}^2 / \rho a$	Magnetic parameter
R_d	$16\sigma^* T_\infty{}^3 / 3kk^*$	Radiation parameter
Re	$aR_1{}^2 / v$	Reynolds number
N_t	$\tau D_B \Delta T / v T_\infty$	Thermophoretic parameter
Pe	bW_c / D_m	Peclet number
Pr	v / α_1	Prandtl number
E	E_a / kT_∞	Activation energy parameter
Le	α_1 / D_B	Lewis number
L_b	v / D_m	Bioconvection Lewis number
δ	$n_\infty / n_w - n_\infty$	Microorganism difference parameter
N_r	$\dfrac{(C_w - C_\infty)(\rho_p - \rho_f)}{\beta \rho_f (T_w - T_\infty)}$	Buoyancy ratio factor
Ω	$T_w - T_\infty / T_\infty$	Temperature ratio parameter
Γ	$K_c{}^2 / 2a$	Chemical reaction parameter
λ	$\dfrac{\beta g(1 - C_f)(T_w - T_0)R_1{}^2}{8 v a z}$	Mixed convection parameter
R_b	$\dfrac{\gamma(n_w - n_\infty)(\rho_m - \rho_f)}{\beta \rho_f (T_w - T_\infty)(1 - C_\infty)}$	Bioconvection Rayleigh number
β_1	$\lambda_1 a$	Maxwell parameter
Fr	$F / R_1 \sqrt{k^*}$	Inertia parameter
K	v / k^*	Porosity parameter

the double-phase flow of the dusty fluid with the hybrid nanofluid past an extending cylinder and have revealed that an upsurge in mass concentration has declined the fluid motion and thermal gradient. Benaziza et al. [28] studied the production of irreversibility amid two coaxial cylinders using an improved ADM for the solution of modeled equations. Eid et al. [29] used blood-based single-walled carbon nanotube (SWCNT) nanofluid past a cylinder immersed by a permeable medium with the effects of EMHD radiations and have concluded that due to the SWCNT flow, thermal distributions have been augmented. Jamshed et al. [30] explored the MHD-mixed convection nanoparticle flow through a vented cavity with an inner elliptic cylinder. Punith et al. [31] scrutinized the Darcy–Forchheimer dusty hybrid nanofluid flow past a cylinder and have concluded that the growth in the fluid motion interaction factor has declined the gradient in velocity for the fluid phase and upsurge velocity for the dust phase. Khan et al. [32] observed the output of convective heat transmission upon the nanofluid flow over a stretching cylinder. It has been highlighted in this study that the Deborah number has augmented the flow and has declined the heat transfer rate.

A medium that contains pores or void spaces in it is termed as a porous medium, and its examples include rubber, wood, and some rocks. A number of porous media are available naturally, but they can also be fabricated. There are abundant applications of porous medium at the industrial level such as filtration and purification processes, seepage of water in sand beds, and drying of porous material in the textile industry. These attractive uses have fascinated the attention of various researchers and scientists. In light of the Darcy Law, the flow of fluid depends linearly upon the pressure gradient and gravitational force. Whenever the porous medium is packed closely, then this law supports the equation of motion for Newtonian fluids with small values of Reynolds number. But for larger pores in the medium, there will be large void spaces in it that leads to viscous shear in addition to Darcy confrontation. In light of this study, P. Forchheimer [33] comprehended the concept of Darcy and has included the square of the flow term in the flow equation for evaluating the inertial forces. Later, Muskat [34] named this term as the Forchhiemer term. Subsequently, many studies have been conducted through porous media by various investigators by focusing on the transmission of heat and mass with different flow conditions. Pandey and Kumar [35] discussed the influence of heat radiation with natural convection upon nanofluids flowing on the stretched cylinder and porous surface. Benos et al. [36] explored the natural convective MHD fluid flow over a saturated permeable enclosure. Redouane et al. [37] inspected the influences of irreversibility upon MHD hybrid nanoparticles through a rotary cylinder subjected to the Brinkman–Forchheimer model and have concluded that augmentation in Darcy and Rayleigh numbers has caused an upsurge in the values of thermal flow convection in the surrounding area of enclosure.

In the Universe, most of the physical problems when modeled mathematically are transformed to the non-linear form. The determination of the exact solution for such problems is very difficult, rather sometimes it is impossible to solve these non-linear problems. So
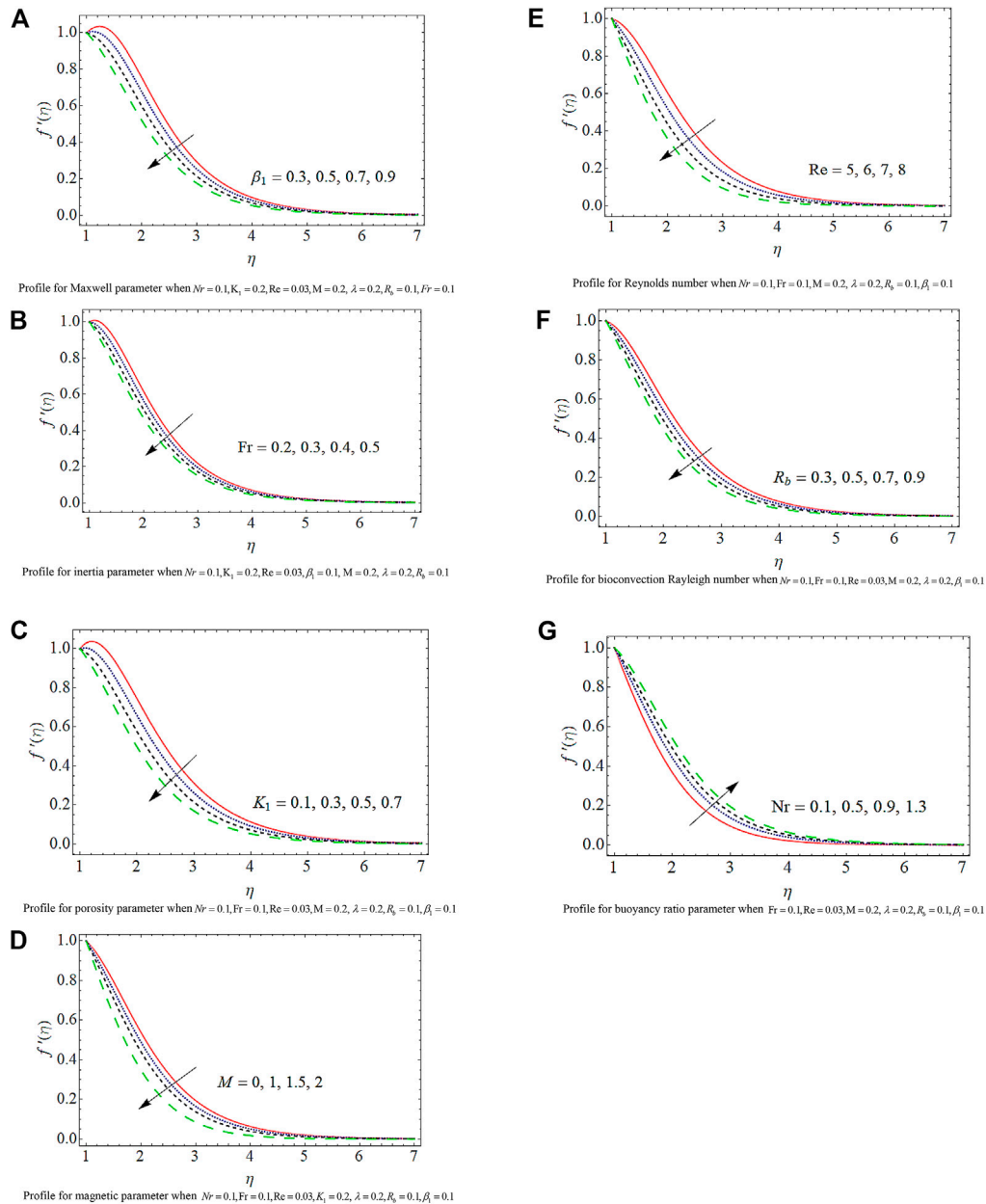
FIGURE 2
Flow profiles under the impact of various substantial parameters.

these problems can be solved by employing either a numerical or semi-numerical technique. In the current investigation, a semi-numerical technique homotopy analysis method (HAM) [38, 39] has been used to determine the solution to modeled problems in a dimensionless form.

Novelty/originality

From the aforementioned works, it was perceived that many examinations have been conducted with the main focus upon heat and mass transfer over a stretching cylinder, but very few examinations have been conducted with the bioconvection MHD fluid flowing upon a stretching cylinder. However, no work has yet been established for Maxwell nanofluid over a stretching and revolving cylinder that is inserted in a permeable medium with the bioconvective phenomenon, which is the main novelty of the current study. The novelty of this work has improved further by exposing the flow system to the coupled effects of chemically reactive Arrhenius activation energy. Moreover, the magnetic effect with B_0 as strength is practiced to the flow system. Additionally, the thermophoretic and Brownian motion characteristics due to the nanofluid flow are captured by implementing the Buongiorno model. The main focus of this work is to discover and to improve the heat and mass transfer for a flow system accompanied by gyrotactic microorganisms.
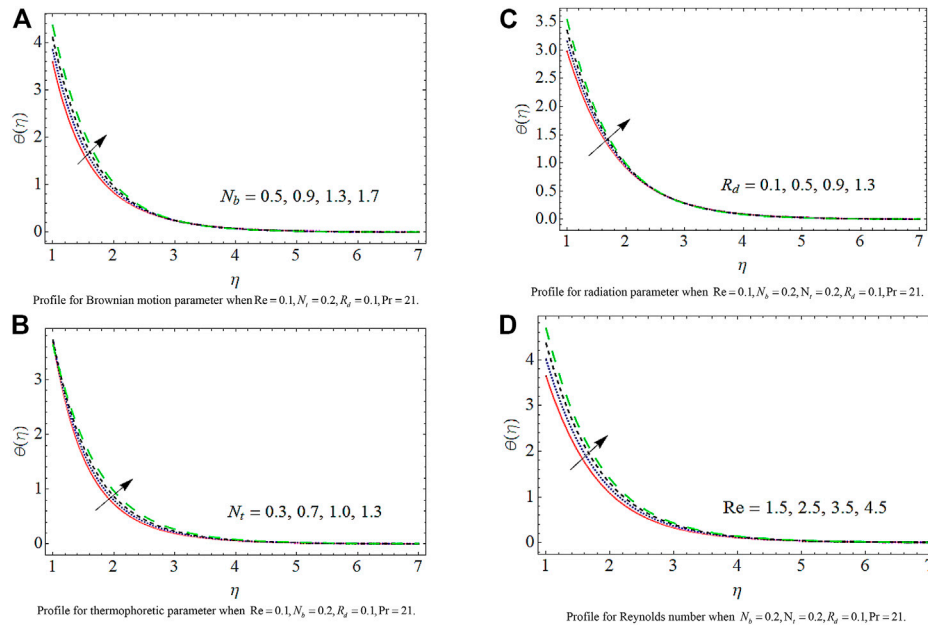
FIGURE 3
Temperature profiles under the impact of various substantial parameters.

The first section of the manuscript includes the literature review and the novelty of the current work. The second section includes the description of the investigation both physically and mathematically. All parameters encountered in this investigation have been defined in this section. The third section comprises the solution technique and its algorithm. The fourth section includes the discussion about different results. A comprehensive detail of the impact of substantial parameters upon different flow profiles has been discussed in this section. In the last section, the main finding has been concluded to give a broader view to the readers.

Physical and mathematical description

Take the bioconvective swirling motion of the Maxwell nanofluid past a stretching cylinder that is inserted in a permeable medium. The following assumptions have been used in this study:

1) The radius of cylinder is assumed to be R_1 that is also performing rotary motion.
2) The magnetic effect with B_0 as the strength is employed to the flow system.
3) To control the thermal effects upon flow, the influence of the heat source, sink, and thermal radiations has been considered.
4) The thermophoretic and Brownian motion characteristics due to the nanofluid flow are captured by implementing the Buongiorno model to the flow system.
5) The $z - axis$ is considered along the axis of the cylinder, while the $r - axis$ is considered along the radial track.
6) The components of velocity in the directions of z, θ and $r-$ axes are u, v and w, respectively.
7) A collective influence of chemically reactive activation energy has also been experienced by the flow system.

8) The microorganism, concentration, and temperature at the cylinder's surface are assumed as n_w, C_w, and T_w, whereas the corresponding values for free stream are n_∞, C_∞, and T_∞ (see Figure 1).

Taking into account the aforementioned assumptions, the resultant equations take the following vector form [40–44]:

$$\nabla.V = 0,$$

$$\rho \frac{dV}{dt} = -\nabla p + \nabla.S - \left(\sigma B_0{}^2 + \frac{v}{k^\star}\right)\frac{u}{\rho} - \frac{1}{\rho\sqrt{k^\star}}F\,u^2$$

$$+ g\left[\frac{1}{\rho_f}\left\{(T - T_\infty)(1 - C_\infty)\beta\rho_f - (C - C_\infty)(\rho_p - \rho_f)\right.\right.$$

$$\left.\left. -\gamma\quad(n - n_\infty)(\rho_m - \rho_f)\quad\right\}\right],$$

$$\frac{dT}{dt} = \tau\left(D_B\nabla C.\nabla T + \frac{D_T}{T_\infty}(\nabla T)^2\right) - \frac{1}{\rho c_p}\nabla.q + \frac{Q_0(T - T_\infty)}{\rho c_p},$$

$$\frac{dC}{dt} - \frac{D_T}{T_\infty}(\nabla T)^2 = -k_r{}^2(C - C_\infty)\left(\frac{T}{T_\infty}\right)^n\exp\left(-\frac{E_a}{k_BT}\right),$$

$$\frac{dn}{dt} + \frac{b\quad W_c}{(C_w - C_\infty)}\ [\nabla(n.\nabla C)] = D_m\,\nabla^2 n. \tag{a}$$

In component notation, we have from the aforementioned equation the following continuity equation,

$$\frac{\partial w}{\partial r} + \frac{w}{r} + \frac{\partial u}{\partial z} = 0, \tag{1}$$

momentum equation,
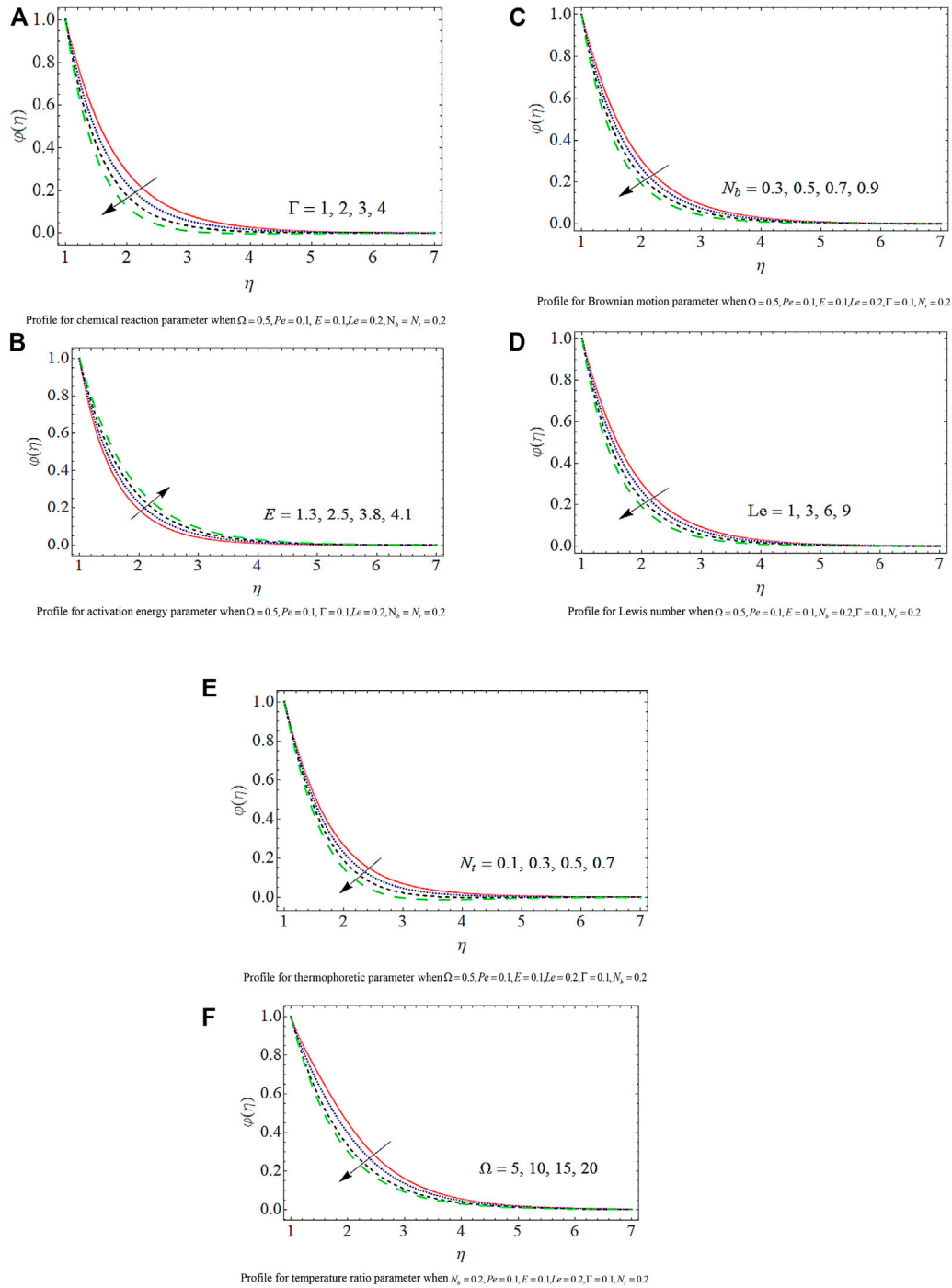
FIGURE 4
Concentration profiles under the impact of various substantial parameters.

$$w \frac{\partial u}{\partial r} + u \frac{\partial u}{\partial z} + \lambda_1 \left[u^2 \frac{\partial^2 u}{\partial z^2} + w^2 \frac{\partial^2 u}{\partial r^2} + 2wu \frac{\partial^2 u}{\partial r \partial w} \right]$$

$$= v \left[\frac{\partial^2 u}{\partial r^2} + \frac{1}{r} \frac{\partial u}{\partial r} \right] - \frac{v}{k^\star} u - \frac{1}{\rho \sqrt{k^\star}} F u^2 - \frac{\sigma B_0^2 u}{\rho}$$

$$+ g \left[\frac{1}{\rho_f} \left\{ (T - T_\infty) \beta \rho_f - (\rho_p - \rho_f)(C - C_\infty) \right. \right.$$

$$\left. \left. - \gamma \quad (n - n_\infty)(\rho_m - \rho_f) \right\} \right], \quad (2)$$

energy equation,

$$u \frac{\partial T}{\partial z} + w \frac{\partial T}{\partial r} = \alpha \left[\frac{\partial^2 T}{\partial r^2} + \frac{\partial T}{\partial r} \frac{1}{r} \right] - \frac{1}{\rho c_P} \frac{1}{r} \frac{\partial (r q_r)}{\partial r}$$

$$+ \tau \left[D_B \frac{\partial C}{\partial r} \frac{\partial T}{\partial r} + \frac{D_T}{T_\infty} \left(\frac{\partial T}{\partial r} \right)^2 \right] + \frac{Q_0}{\rho c_P} (T - T_\infty), \quad (3)$$

concentration equation,

A

$L_b = 0.1, 0.3, 0.6, 0.9$

Profile for bioconvection Lewis number when $\Omega = 0.5, Pe = 0.1, E = 0.1, N_b = N_r = 0.2$

B

$Pe = 0.1, 0.4, 0.7, 1.0$

Profile for Peclet number when $\Omega = 0.5, L_b = 0.1, E = 0.1, N_b = N_r = 0.2$

FIGURE 5
Motile microorganism profiles under the impact of different parameters.
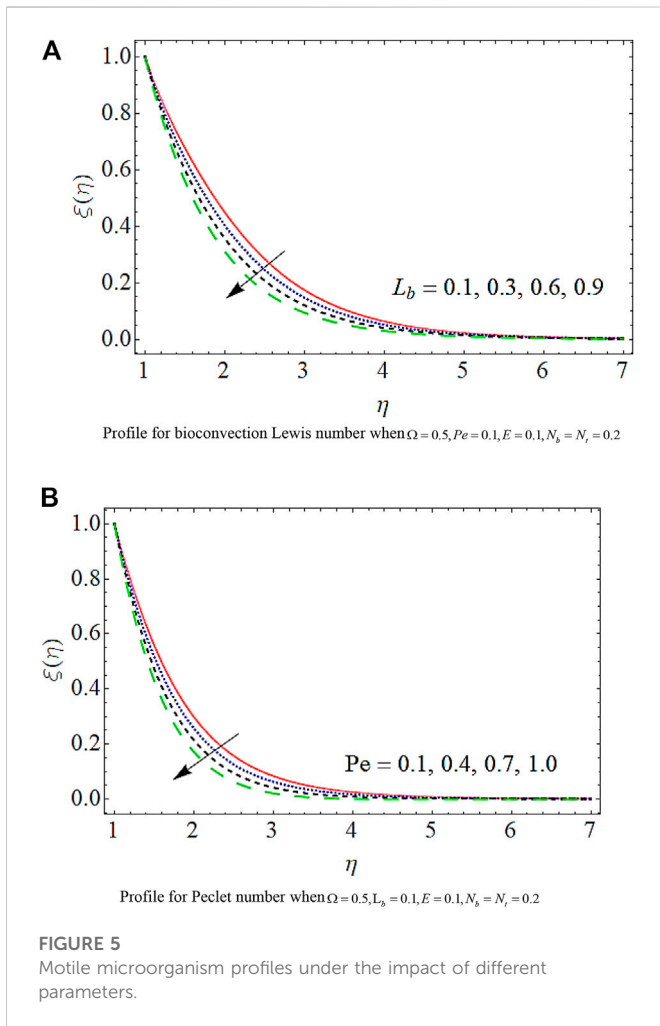
$$u \frac{\partial C}{\partial z} + w \frac{\partial C}{\partial r} = D_B \left[\frac{\partial^2 C}{\partial r^2} + \frac{\partial C}{\partial r} \frac{1}{r} \right] + \frac{D_T}{T_\infty} \left[\frac{\partial T}{\partial r} \frac{1}{r} + \frac{\partial^2 T}{\partial r^2} \right]$$
$$- k_r^2 (C - C_\infty) \left(\frac{T}{T_\infty} \right)^n \exp \left(-\frac{E_a}{k_B T} \right), \quad (4)$$

and gyrotactic microorganism equation,

$$u \frac{\partial n}{\partial z} + w \frac{\partial n}{\partial r} + \frac{b \ W_c}{(C_w - C_\infty)} \left[\frac{\partial}{\partial r} \left(n \frac{\partial C}{\partial r} \right) \right] = D_m \frac{\partial^2 n}{\partial r^2}. \quad (5)$$

The subjected boundary conditions (BCs) are [45, 46]

$$w(r, z) = 0, \ u(r, z) = 2az, -k \frac{\partial T}{\partial r} = h \left(T_f - T \right),$$
$$-D_B \frac{\partial C}{\partial r} = k \left(C_f - C \right), -D_m \frac{\partial n}{\partial r} = h \left(n_f - n \right) \ at \ r = R_1,$$
$$u \to 0, \quad C \to C_\infty, \quad n \to n_\infty, \quad T \to T_\infty, \quad as \quad r \to \infty \quad (6)$$

where D_B and D_T are mass diffusivity and thermophoretic coefficients, α is the thermal diffusivity, D_m is the coefficient of microorganism diffusion, W_c is the speed of the swimming cell, g is the gravity, Q_0 is the heat source coefficient, b is the chemotaxis constant, K_r is the chemical reaction, E_a is the coefficient of activation energy, and B_0 is the strength of the magnetic field.

A group of similar variables is used to obtain a dimensionless form of modeled equations (40) and (43).

$$u = 2az f'(\eta), \quad w = -aR_1 \frac{f(\eta)}{\eta^{1/2}},$$
$$\phi(\eta) = \frac{C - C_\infty}{C_w - C_\infty}, \ \theta(\eta) = \frac{T - T_\infty}{T_w - T_\infty}, \quad \xi(\eta) = \frac{n - n_\infty}{n_w - n_\infty}, \quad (7)$$
$$\eta = \left(\frac{r}{R_1} \right)^2.$$

In light of Eq. 7, we have from Eqs 1–6

$$\eta f''' + f'' - \beta_1 Re \left(\frac{1}{\eta} f'' f^2 + 2f' f''' - 4f \ f' f'' \right) - ReFr f'^2 + Re f f''$$
$$- f' (K_1 + ReM) + \lambda (N_r \varphi + \theta + R_b \xi) = 0, \quad (8)$$

$$(1 + R_d) (\eta \theta'' + \theta') + RePr f \theta' + N_b Pr \eta \varphi' \theta' + N_t Pr \eta \theta'^2 = 0, \quad (9)$$

$$\eta \varphi'' + \varphi' + PrRe Le f \varphi' + Pr Le \frac{N_t}{N_b} \theta'$$
$$+ LePr \frac{N_t}{N_b} \eta \theta'' + \Gamma LePr \varphi (1 + \Omega \theta)^n \exp \left(\frac{-E}{1 + \Omega \theta} \right) = 0, \quad (10)$$

$$2\eta \xi'' + (1 + 2ReL_b f) \xi' - Pe [2\eta \xi' \varphi' + (\xi + \delta) (\varphi' + 2\eta \varphi'')] = 0. \quad (11)$$

Subjected BCs with the help of Eq. 7 become

$$f(1) = 0, \ f'(1) = 1, \quad \theta'(1) = -\varepsilon_1 (1 - \theta(1)), \ \varphi(1) = 1, \quad \xi(1) = 1$$
$$f'(\infty) = 0, \quad \theta(\infty) = 0, \quad \varphi(\infty) = 0, \ \xi(\infty) = 0, \quad (12)$$

where $\varepsilon_1 = \frac{h_t}{k} \sqrt{\frac{v}{a}}$ is the Biot number.

In the process of aforementioned non-dimensionalization, few physical parameters have been obtained which are described in detail in Table 1.

Physical quantities

In thermodynamics, scientists and engineers are basically concerned to explore and determine the heat and mass diffusions for fluid motion. Some interested quantities are discussed as follows:

1) Nusselt number:

$$Nu = \frac{R_1}{k (T_w - T_\infty)} (-k) \left(\frac{\partial T}{\partial r} \right)_{r=R_1}. \quad (13)$$

Incorporating Eq. 7 in Eq. 13, we have

$$Nu = -2\theta'(1). \quad (14)$$

2) Sherwood number:

$$Sh = \frac{R_1}{k (C_w - C_\infty)} (-D_B) \left(\frac{\partial C}{\partial r} \right)_{r=R_1}. \quad (15)$$

Substituting Eq. 7 in Eq. 15, we have

$$Sh = -2\phi'(1). \quad (16)$$
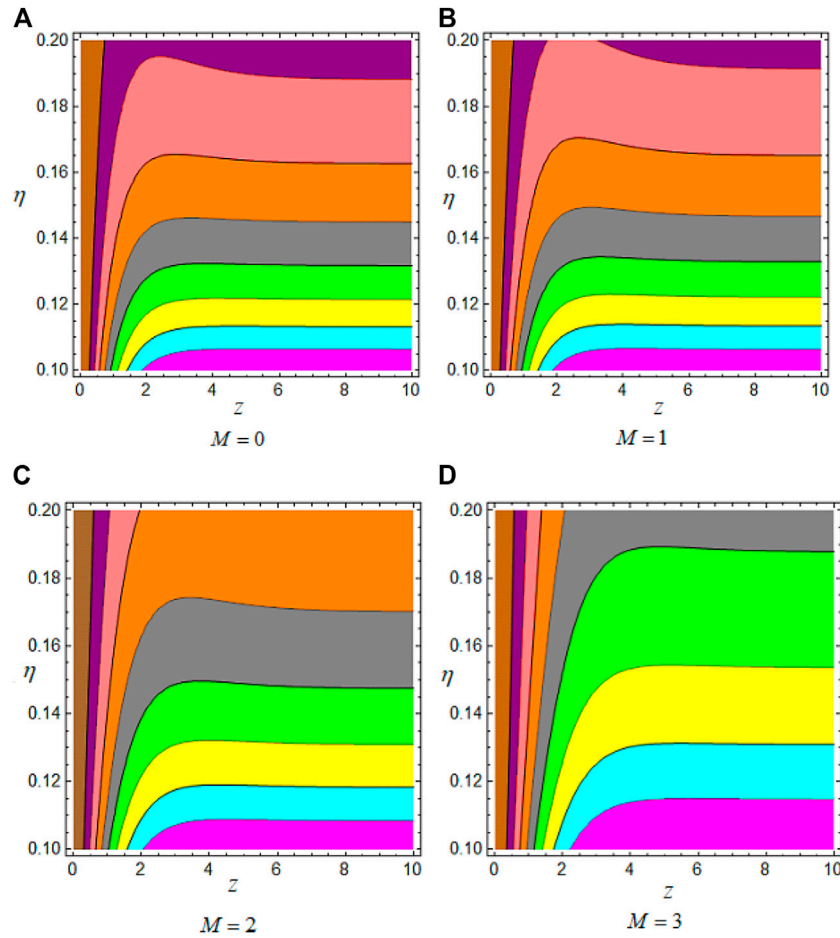
FIGURE 6
(A–D): Impact of the magnetic field on streamlines when $Fr = 0.1$, $\lambda = 0.2$, $R_b = 0.1$, $\beta_1 = 0.1$.

3) Microorganism density number:

$$Nn = \frac{R_1}{D_m (N_w - N_\infty)} (-D_m) \left(\frac{\partial N}{\partial r} \right)_{r = R_1}. \tag{17}$$

Substituting Eq. 7 in Eq. 17, we get

$$Nn = -2\xi_n(1). \tag{18}$$

Solution method

The governing equations have changed to dimensionless notations with suitable variables. The obtained set of dimensionless Eqs 8–11 in light of boundary conditions given in Eq. 12 will now be solved using HAM. This technique requires some initial guesses as startup values, which are given as follows:

$$f_0(\eta) = \frac{1}{1 + \alpha(1 + K_1)} (1 - e^\eta), \quad \Theta_0(\eta) = (1 - \gamma) e^{-\eta},$$
$$\Phi_0(\eta) = (1 - \gamma_1)e^{-\eta}, \quad \xi(\eta) = (1 - \gamma_2)e^{-\eta}. \tag{19}$$

The linear operators are as follows:

$$L_f = f''' - f', \quad L_\Theta = \theta'' - \theta, \quad L_\Phi = \phi'' - \phi, \quad L_\xi = \xi'' - \xi. \tag{20}$$

Furthermore,

$$L_f (S_1 + S_2 e^\eta + S_3 e^{-\eta}) = 0, \quad L_\Theta (S_4 e^\eta + S_5 e^{-\eta}) = 0,$$
$$L_\Phi (S_6 e^\eta + S_7 e^{-\eta}) = 0, \quad L_\xi (S_8 e^\eta + e S_9 e^{-\eta}) = 0, \tag{21}$$

where S_i for $i = 1, 2, 3.......9$ are fixed values.

$$N_{\widehat{f}} \left[\widehat{f}(\eta \; ; \; \xi), \quad \widehat{\theta}(\eta \; ; \; \xi), \widehat{\phi}(\eta \; ; \; \xi), \widehat{\xi}(\eta \; ; \; \xi) \right]$$
$$= \widehat{f}_{\eta\eta} + \eta \widehat{f}_{\eta\eta\eta} - \beta_1 \mathrm{Re} \left(\frac{1}{\eta} \left(\widehat{f} \right)^2 \widehat{f}_{\eta\eta} + 2 \widehat{f}_\eta \widehat{f}_{\eta\eta\eta} - 4 \widehat{f} \widehat{f}_\eta \widehat{f}_{\eta\eta} \right)$$
$$- \mathrm{Re} \left(\widehat{f}_\eta \right)^2 + \mathrm{Re} \widehat{f} \widehat{f}_{\eta\eta} - (K_1 + \mathrm{Re}M) \widehat{f}_\eta + \lambda \left(\widehat{\theta} + N_r \widehat{\varphi} + R_b \widehat{\xi} \right), \tag{22}$$

$$N_{\widehat{\theta}} \left[\widehat{f}(\eta;\xi), \widehat{\theta}(\eta;\xi), \widehat{\phi}(\eta;\xi), \widehat{\xi}(\eta;\xi) \right]$$
$$= (1 + R_d) \left(\eta \widehat{\theta}_{\eta\eta} + \widehat{\theta}_\eta \right) + \mathrm{PrRe} \widehat{f} \widehat{\theta}_\eta + N_b \mathrm{Pr} \, \eta \widehat{\phi}_\eta \widehat{\theta}_\eta + N_t \eta \mathrm{Pr} \left(\widehat{\theta}_\eta \right)^2, \tag{23}$$
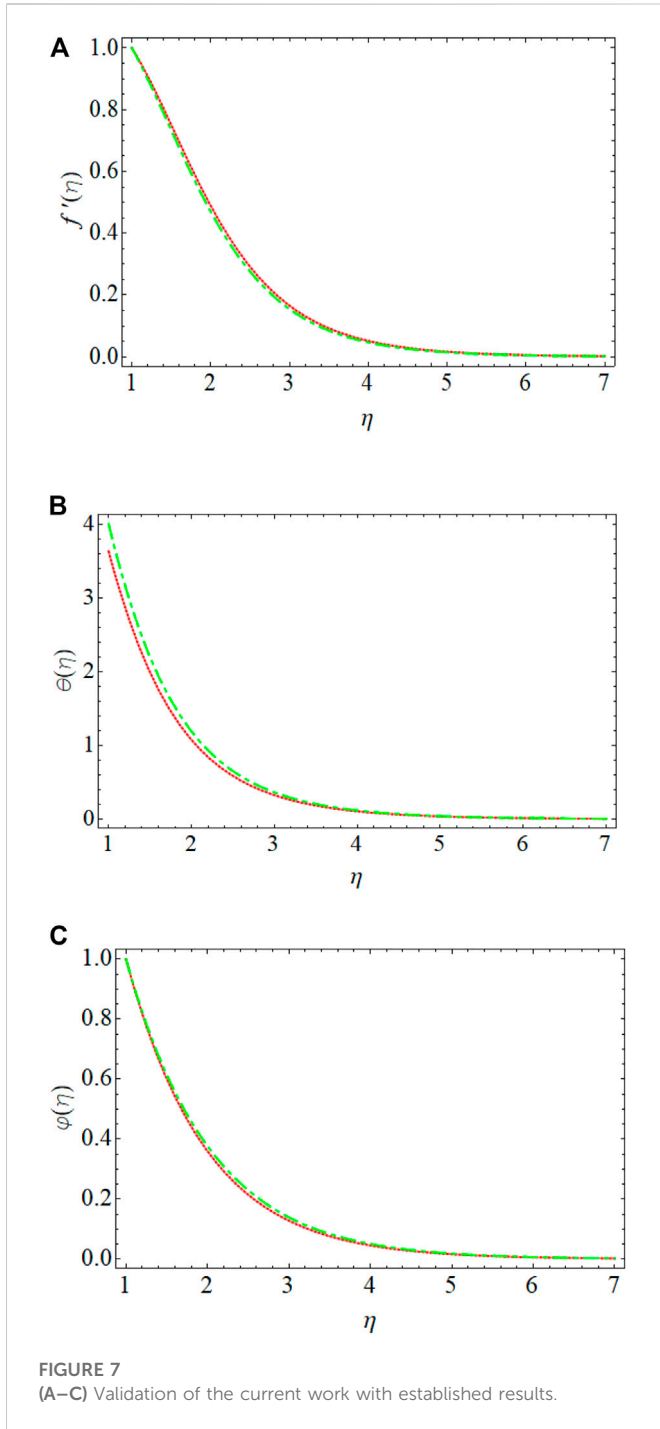
FIGURE 7
(A–C) Validation of the current work with established results.

$$N_{\widehat{\phi}}\Big[\widehat{f}(\eta;\xi),\widehat{\theta}(\eta;\xi),\widehat{\phi}(\eta;\xi),\widehat{\xi}(\eta;\xi)\Big]$$
$$= \eta\widehat{\phi}_{\eta\eta} + \widehat{\phi}_{\eta} + PrLe\left(Re\widehat{f}\widehat{\phi}_{\eta} + \frac{N_t}{N_b}\widehat{\theta}_{\eta\eta}\right)$$
$$+ LePr\,\Gamma\widehat{\phi}\Big(1 + \Omega\widehat{\theta}\Big)^n \exp\left(\frac{-E}{1 + \Omega\widehat{\theta}}\right), \qquad (24)$$

$$N_{\widehat{\xi}}\Big[\widehat{f}(\eta;\xi),\widehat{\theta}(\eta;\xi),\widehat{\phi}(\eta;\xi),\widehat{\xi}(\eta;\xi)\Big]$$
$$= 2\eta\widehat{\xi}_{\eta\eta} + \Big(1 + 2Re L_b\widehat{f}\Big)\widehat{\xi}_{\eta} - Pe\Big[2\eta\widehat{\xi}_{\eta}\widehat{\phi}_{\eta} + \Big(\delta + \widehat{\xi}\Big)\Big(\widehat{\phi}_{\eta} + 2\eta\widehat{\phi}_{\eta\eta}\Big)\Big]. \qquad (25)$$

The 0-order description for Eqs 8–11 is given as follows:

$$(1 - \zeta)L_{\widehat{f}}\Big[\widehat{f}(\eta;\zeta) - \widehat{f}_0(\eta)\Big] = \zeta\hbar_{\widehat{f}}N_{\widehat{f}}\Big[\widehat{f}(\eta;\xi),\widehat{\theta}(\eta;\xi),\widehat{\phi}(\eta;\xi),$$
$$\widehat{\xi}(\eta;\xi|])\Big], \qquad (26)$$

$$(1 - \zeta)L_{\widehat{\theta}}\Big[\widehat{\theta}(\eta;\zeta) - \widehat{\theta}_0(\eta)\Big] = \zeta\hbar_{\widehat{\theta}}N_{\widehat{\theta}}\Big[\widehat{f}(\eta;\xi),\widehat{\theta}(\eta;\xi),\widehat{\phi}(\eta;\xi),$$
$$\widehat{\xi}(\eta;\xi)\Big], \qquad (27)$$

$$(1 - \zeta)L_{\widehat{\phi}}\Big[\widehat{\phi}(\eta;\zeta) - \widehat{\phi}_0(\eta)\Big] = \zeta\hbar_{\widehat{\phi}}N_{\widehat{\phi}}\Big[\widehat{f}(\eta;\xi),\widehat{\theta}(\eta;\xi),\widehat{\phi}(\eta;\xi),$$
$$\widehat{\xi}(\eta;\xi)\Big], \qquad (28)$$

$$(1 - \zeta)L_{\widehat{\xi}}\Big[\widehat{\xi}(\eta;\zeta) - \widehat{\xi}_0(\eta)\Big] = \zeta\hbar_{\widehat{\xi}}N_{\widehat{\xi}}\Big[\widehat{f}(\eta;\xi),\widehat{\theta}(\eta;\xi),\widehat{\phi}(\eta;\xi),\widehat{\xi}(\eta;\xi)\Big]. \qquad (29)$$

Related conditions are as follows:

$$\widehat{f}(\eta;\zeta)\Big|_{\eta=1} = 0, \left.\frac{\partial\widehat{f}(\eta;\zeta)}{\partial\eta}\right|_{\eta=1} = 1,$$
$$\widehat{\theta}(\eta;\zeta)\Big|_{\eta=1} = -\varepsilon_1\Big(1 - \widehat{\theta}(1)\Big), \widehat{\phi}(\eta;\zeta)\Big|_{\eta=1} = 1,$$
$$\widehat{\xi}(\eta;\zeta)\Big|_{\eta=1} = 1 \left.\frac{\partial\widehat{f}(\eta;\zeta)}{\partial\eta}\right|_{\eta\to\infty} = 0, \qquad (30)$$
$$\widehat{\phi}(\eta;\zeta)\Big|_{\eta\to\infty} = 0, \widehat{\xi}(\eta;\zeta)\Big|_{\eta\to\infty} = 0, \widehat{\theta}(\eta;\zeta)\Big|_{\eta\to\infty} = 0,$$

such that $\zeta \in [0,\ 1]$, so for $\zeta = 0$ *and* $\zeta = 1$, we have

$$\widehat{f}(\eta;1) = \widehat{f}(\eta), \quad \widehat{\theta}(\eta;1) = \widehat{\theta}(\eta), \quad \widehat{\xi}(\eta;1) = \widehat{\xi}(\eta), \widehat{\phi}(\eta;1) = \widehat{\phi}(\eta). \qquad (31)$$

The Taylor's series expansion for $\widehat{f}(\eta;\zeta)$, $\widehat{\theta}(\eta;\zeta)$, $\widehat{\phi}(\eta;\zeta)$, and $\widehat{\xi}(\eta;\zeta)$ around $\zeta = 0$

$$\widehat{f}(\eta;\zeta) = \widehat{f}_0(\eta) + \sum_{n=1}^{\infty}\widehat{f}_n(\eta)\zeta^n,$$
$$\widehat{\phi}(\eta;\zeta) = \widehat{\phi}_0(\eta) + \sum_{n=1}^{\infty}\widehat{\phi}_n(\eta)\zeta^n,$$
$$\widehat{\theta}(\eta;\zeta) = \widehat{\theta}_0(\eta) + \sum_{n=1}^{\infty}\widehat{\theta}_n(\eta)\zeta^n, \qquad (32)$$
$$\widehat{\xi}(\eta;\zeta) = \widehat{\xi}_0(\eta) + \sum_{n=1}^{\infty}\widehat{\xi}_n(\eta)\zeta^n,$$

$$\widehat{f}_n(\eta) = \frac{1}{n!}\left.\frac{\partial\widehat{f}(\eta;\zeta)}{\partial\eta}\right|_{p=0}, \widehat{\theta}_n(\eta) = \frac{1}{n!}\left.\frac{\partial\widehat{\theta}(\eta;\zeta)}{\partial\eta}\right|_{p=0},$$
$$\widehat{\phi}_n(\eta) = \frac{1}{n!}\left.\frac{\partial\widehat{\phi}(\eta;\zeta)}{\partial\eta}\right|_{p=0}, \widehat{\xi}_n(\eta) = \frac{1}{n!}\left.\frac{\partial\widehat{\xi}(\eta;\zeta)}{\partial\eta}\right|_{p=0}. \qquad (33)$$

Related BCs are as follows:

$$\widehat{f}(1) = 0, \widehat{f}'(1) = 1, \widehat{\theta}'(1) = -\varepsilon_1\Big(1 - \widehat{\theta}(1)\Big), \widehat{\phi}(1) = 1,$$
$$\widehat{\xi}(1) = 1, \widehat{f}'(\infty) = 0, \widehat{\theta}(\infty) = 0, \widehat{\phi}(\infty) = 0, \widehat{\xi}(\infty) = 0. \qquad (34)$$

Then, we have

TABLE 2 Skin friction $C_{fx}Re_x^{0.5}$ vs. various parameters for the Maxwell nanofluid.

Re	K_1	β_1	M	Fr	λ	Nr	Rb	Cf_x
0.1	0.1	0.1	0.1	0.1	0.1	0.1	0.1	0.875568097 55
0.2								0.886579198224
0.3								0.896689299124
	0.2							0.912432217421
	0.3							0.923421323521
		0.2						0.933523605131
		0.3						0.944021322142
			0.2					0.962133023141
			0.3					0.978863214210
				0.2				0.983421567902
				0.3				0.992132134110
					0.2			1.012321132143
					0.3			1.112213245467
						0.2		1.003215743213
						0.3		0.972243189021
							0.2	0.973421567654
							0.3	0.984532765432

TABLE 3 Nusselt number $Nu_x Re_x^{-0.5}$ against numerous factors.

Nb	Nt	Rd	Re	Nu_x
0.1	0.1	0.1	0.1	3.123127642101
0.2				3.124238652212
0.3				3.125348762321
	0.2			3.137213452134
	0.3			3.148324562331
		0.2		3.202314324211
		0.3		3.422134231554
			0.2	3.221233142317
			0.3	3.022876452315
				2.875643885322
				2.632125432144

$$\mathfrak{R}_n^{\widehat{f}}(\eta) = \eta\widehat{f}_{n-1}''' + \widehat{f}_{n-1}'' - \beta_1 \operatorname{Re}\left(\frac{1}{\eta}\left(\widehat{f}_{n-1}\right)^2 \widehat{f}_{n-1}'' + 2\widehat{f}_{n-1}'\widehat{f}_{n-1}''' - 4\widehat{f}\sum_{j=0}^{w-1}\widehat{f}_{w-1-j}\widehat{f}_j''\right)$$
$$- \operatorname{Re}\left(\widehat{f}_{n-1}'\right)^2 + \operatorname{Re}\widehat{f}\sum_{j=0}^{w-1}\widehat{f}_{w-1-j}\widehat{f}_j'' - (K_1 + \operatorname{Re}M)\widehat{f}_{n-1}'$$
$$+ \lambda\left(\widehat{\theta}_{n-1} + N_r\widehat{\varphi}_{n-1} + R_b\widehat{\xi}_{n-1}\right),$$

$$(35)$$

$$\mathfrak{R}_n^{\widehat{\theta}}(\eta) = (1 + R_d)\left(\widehat{\theta}_{n-1}'' + \widehat{\phi}_{n-1}'\right)$$
$$+ \operatorname{Pr}\left(\operatorname{Re}\sum_{j=0}^{w-1}\widehat{\theta}_{n-1}'\widehat{f}_{w-1-j} + \eta\left(N_b\widehat{\theta}_{n-1}'\widehat{\phi}_{n-1}' + N_t\left(\widehat{\theta}_{n-1}'\right)^2\right)\right), \quad (36)$$

$$\mathfrak{R}_n^{\widehat{\phi}}(\eta) = \eta\widehat{\phi}_{n-1}'' + \widehat{\phi}_{n-1}' + \operatorname{Pr}Le\left(\operatorname{Re}\widehat{f}\widehat{\phi}_{\eta-1} + \frac{N_t}{N_b}\widehat{\theta}''_{n-1}\right)$$
$$+ LePr\Gamma\left(1 + \Omega\widehat{\theta}\right)^n \exp\left(\frac{-E}{1+\Omega\widehat{\theta}}\right)\sum_{j=0}^{w-1}\phi_{w-1-j}, \quad (37)$$

$$\mathfrak{R}_n^{\widehat{\xi}}(\eta) = 2\eta\widehat{\xi}_{n-1}'' + \sum_{j=0}^{w-1}\left(1 + 2\operatorname{Re}L_b\widehat{f}_j\right)\widehat{\xi}_{w-1-j}'$$
$$- Pe\left(\sum_{j=0}^{w-1}\widehat{\xi}_{w-1-j}'\widehat{\phi}_j + \sum_{j=0}^{w-1}\left(\delta + \widehat{\xi}_{w-1-j}\right)\left(\widehat{\phi}_{n-1}' + 2\eta\widehat{\phi}_{n-1}''\right)\right),$$

$$(38)$$

TABLE 4 Sherwood number against different factors for the Maxwell nanofluid.

Re	Nt	Nb	Le	Γ	Ω	n	Sh_x
0.1	0.1	0.1	0.1	0.1	0.1	1	1.2032041231
0.2							1.2142132433
0.3							1.2243217865
	0.2						1.2543342112
	0.3						1.2642138076
		0.2					1.2356431278
		0.3					1.2032154321
			0.2				1.1802364220
			0.3				1.1622453321
				0.2			1.1623256787
				0.3			1.1625679843
					0.2		1.1613210231
					0.3		1.6121013210
						2	1.6432256442
						3	1.6765482103

TABLE 5 Motile rate _vs._ the embedded parameters for the Maxwell nanofluid.

Re	Pe	Lb	δ	$\xi'(1)$
0.1	0.1	0.1	0.1	1.3143152342
0.2				1.3254327643
0.3				1.3334210765
	0.2			1.3425433421
	0.3			1.3626421380
		0.2		1.3823564312
		0.3		1.4020321543
			0.2	1.4118023642
			0.3	1.4216224533

Moreover, we have $\xi_n = \begin{cases} 0, & \text{if } \zeta \le 1 \\ 1, & \text{if } \zeta > 1. \end{cases}$ (39)

Discussion of results

This work examines the effects of the bioconvection Maxwell nanofluid flow over a stretching and revolving cylinder that is inserted in a permeable medium. The thermophoretic and Brownian motion characteristics due to the nanofluid flow are captured by implementing the Buongiorno model. The core importance of this study is to explore and improve the thermal and mass transmission for the flow system. The influence of various

parameters with numerical values $Nr = 0.1$, $K_1 = 0.2$, $Re = 0.03$, $\beta_1 = 0.1$, $\lambda = 0.2$, $R_b = 0.1$, $N_b = 0.2$, $N_t = 0.2$, $R_d = 0.1$, $Fr = 0.01$, $Le = 0.4$, $\Gamma = 0.5$, $\Omega = 0.5$, $L_b = 0.1$, $\delta = 0.2$, $Pe = 0.1$, $M = 0.3$, $Pr = 21$ on fluid flow will be described theoretically with the help of graphical view in the upcoming paragraphs.

Figure 2 describes the effect of different parameters on the velocity of the fluid. Figure 2A depicts that augmenting values of the Maxwell parameter β_1 declines fluid flow. Basically, the growing values of β_1 enhance the stress relaxation phenomenon, which drops down the flow characteristics, as depicted in Figure 2A. From Figure 2B, it has been noticed that the inertia coefficient or Forchheimer number Fr has an adverse impact upon the velocity of the fluid. The upper values of Fr cause a decline in the flow profile. Since an augmentation in Fr
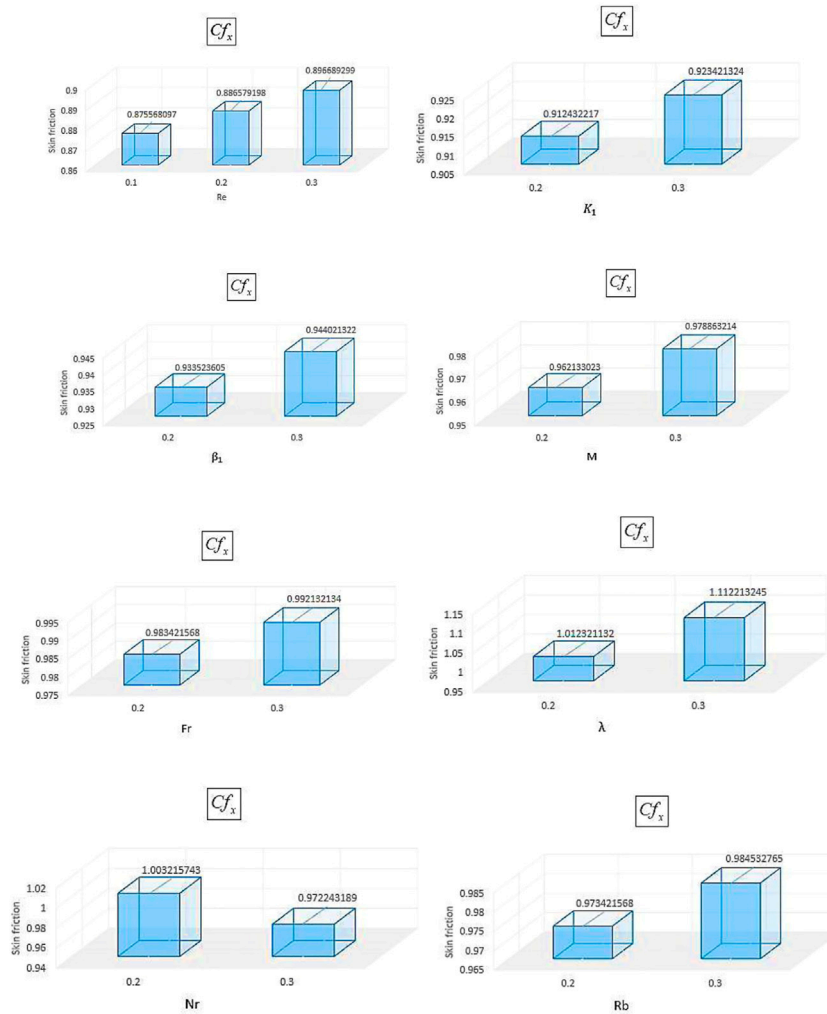
CHART 1
Statistical calculation for skin friction $C_{fx}Re_x^{0.5}$ against numerous factors.

causes the generation of higher resistive or drag forces to the flow of the fluid, this physical phenomenon results in a decline in the profile of fluid flow. The motion of fluid, as depicted in Figure 2C, reduces for a growth in the porosity parameter K_1. For growth in K_1, the void spaces in the medium increase, and this offers more conflict to the fluid motion and gradually causes a decline in the flow profiles. Figure 2D portrays the magnetic impacts M upon flow. The Lorentz force is generated for augmenting the values of M, which offers a resistance to the flow and causes reduction in the flow characteristics. Therefore, the magnetic effect significantly monitors the flow behavior of fluid particles. Figure 2E depicts the impact of the Reynolds number Re upon the flow profile. The inertial force is a conflicting agent to the flow of fluid particles, where this inertial force within the fluid particles becomes dominant with a growth in Re, which opposes the fluid motion. Hence, the augmenting values of Re reduce the flow profile, as presented in Figure 2E. The impact of the bioconvection number R_b is depicted in Figure 2F. Physically, an augmentation in R_b creates a contrasting force to the fluid particles in the direction of motion that leads to a reduction in the flow profile. Figure 2G depicts that strength of the momentum boundary layer rises

up with enhancing values of N_r. Hence, the velocity profile grows up for higher values of N_r.

Figure 3A portrays the influence of N_b upon the thermal profile. Physically, when the values of N_b increase higher, then the haphazard flow of fluid particles also increases for which the collision among the fluid particles increases. In this phenomenon, kinetic energy of the fluid particles is changed to thermal energy, which results ultimately in augmentation in the thermal characteristics of particles. The effect of the thermophoretic parameter N_t upon heat flow is depicted in Figure 3B. From this figure, it has been revealed that, for an upsurge in N_t, there is a higher difference in the temperature that will lead to a growth in the temperature flow from a warmer region to a colder region. This physical phenomenon results in augmentation in the temperature of the fluid. Figure 3C endorses that thermal diffusion is supported by a growth in the radiation parameter R_d. Physically, an augmentation in R_d increases the size of the thermal boundary layer and diffuses more heat. Hence, the higher values of R_d provide maximum temperature to the flow system. Figure 3D illustrates the effect of Reynolds number Re on the thermal profile. It is obvious from this figure
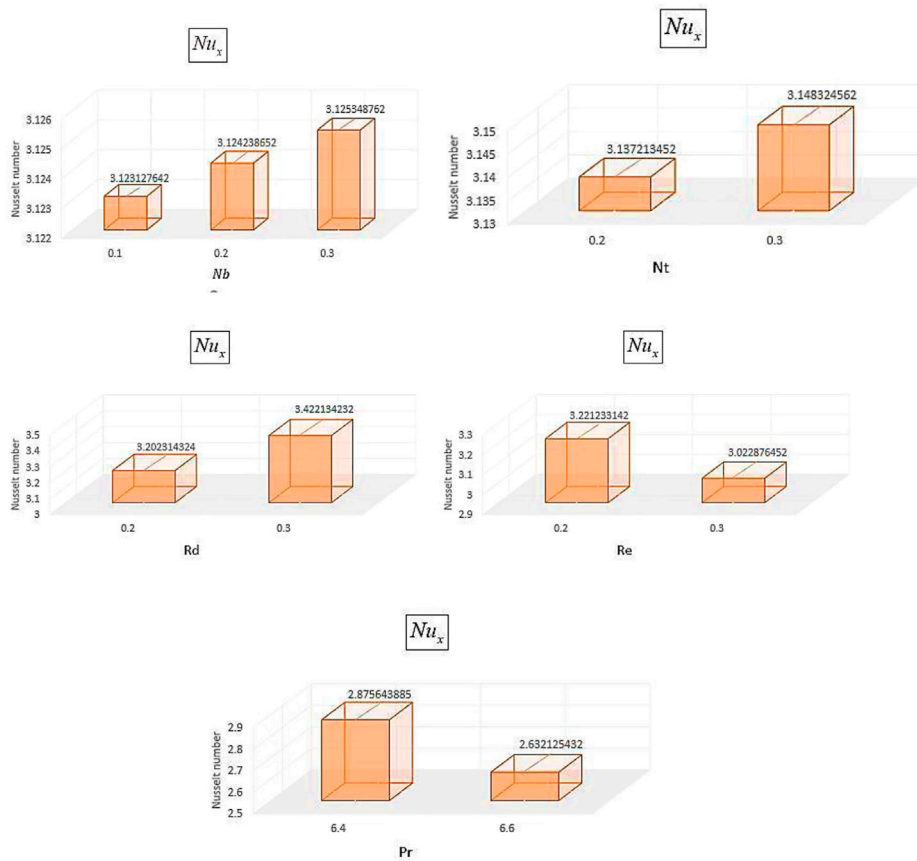
CHART 2
Statistical calculation for the Nusselt number $Nu_x Re_x^{-0.5}$ against numerous factors.

that more thermal flow occurs for growth in Re. The fluid's convective force declines for augmentation in Re, which boosts up the thermal boundary layer wideness and causes a growth in temperature.

Figure 4 shows the influence of different physical parameters over concentration. Figure 4A portrays that the width of the concentration border line declines with the augmenting values of the chemical reaction parameter Γ. With the augmentation in Γ, the fluid molecular diffusivity shrinks, for which less mass transfer occurs. In this phenomenon, the concentration of the fluid drops down as values of Γ increase. With the augmentation in the activation energy factor E, the concentration characteristics increase, as depicted in Figure 4B. Physically, the number of fluid molecules with a requirement of small energy is enhanced for growing values of E, which result in more mass diffusion. Figure 4C shows that with the augmentation in N_b, the concentration profiles upsurge. When N_b increases, then the random collision among the fluid particles also increases, which leads to a reduction in mass transfer. Hence, growth in N_b resembles a decline in the concentration characteristics. The impact of Lewis number upon mass flow is depicted in Figure 4D. With the growth in Le, the mass flow declines that weakens the concentration characteristics. Mass flow is also depreciated with the augmentation in N_t, as depicted in Figure 4E. The thermal conductivity of the fluid improves with the progression in N_t that

weakens the strength of the concentration boundary layer, due to which less mass transmission takes place. Figure 4F depicts that concentration is a reducing function of the temperature ratio parameter Ω. Since the growing values of Ω result in an augmentation in the temperature difference that leads to more thermal flow at the free stream. In this physical phenomenon, the mass flow in the closed neighborhood of the cylinder reduces, which declines the concentration. Hence, growth in the values of Ω corresponds to a decline in the concentration, as shown in Figure 4F.

The impact upon the density of motile microorganisms for variations in L_b and Pe is described in Figure 5. This figure confirms that the density of microorganism declines with the growth in L_b and Pe. The augmenting values of L_b cause degeneration in the motile microorganism density, which leads to reduction in the distribution of motile microorganisms, as shown in Figure 5A. The Peclet number Pe is closely related to microorganism diffusivity. It is observed that the greater values of Pe cause a decline in diffusion of motile microorganisms. Hence, augmenting values of Pe decline the profile for motile microorganisms, as presented in Figure 5B. Figures 6A–D display the magnetic effects M in the form of streamlines. The variations in streamlines have been rapidly shown with the increasing amount of the magnetic parameter.

CHART 3
Statistical calculation for the motile rate $\xi'(1)$ vs. various parameters
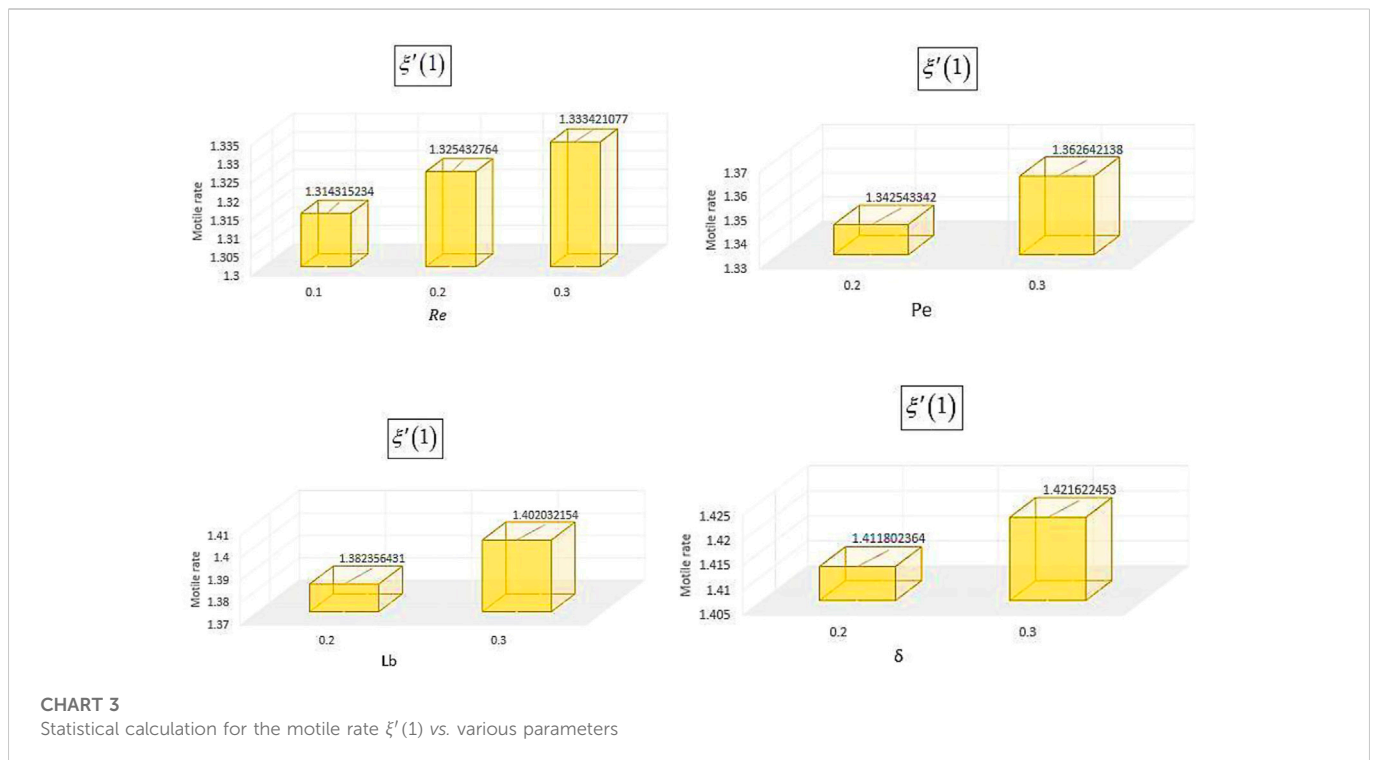
Figures 7A–C depict the authentication of this work. In this figure, the current results are endorsed with the established work given by Ahmed et al. [42] by taking the common factors. This figure recommends a closed settlement between the published and current work.

Discussion of tables

The impact of different emerging factors over interested quantities has been numerically described in Table 2, Table 3, Table 4, and Table 5. Table 2 portrays that the skin friction grows up in response to the resistive force produced by the augmenting values of the Maxwell parameter, inertia coefficient, porosity parameter, magnetic parameter, Reynolds number, and bioconvection Rayleigh number, while it decays with the growth in the buoyancy ratio parameter. The statistical calculations for skin friction in response to different parameters are presented in Chart 1. Table 3 portrays that the heat flow rate upsurges for augmentation in Brownian motion, thermophoretic parameter, Reynolds number, and radiation parameter. The thermal flow rate vs. different parameters is statistically given in Chart 2. The mass flow rate is supported by the growth in the activation energy parameter, while it is opposed by the augmentation in the chemical parameter, Lewis number, thermophoretic parameter, and temperature ratio parameter, as depicted numerically in Table 4. The density number of microorganisms is declined by a growth in the values of Peclet and bioconvective Lewis numbers, as presented in Table 5, while its statistical calculations are presented in Chart 3.

Conclusion

This work determines the bioconvection Maxwell nanofluid flow over a stretching and revolving cylinder that is inserted in a permeable medium. The main focus of this work is to explore and improve thermal and mass transmission for the flow system. The thermophoretic and Brownian motion characteristics due to the nanofluid flow are captured by implementing the Buongiorno model. After deep inspection of the current study, the following main points are concluded:

1) With the growth in values of the Maxwell parameter, inertia coefficient, bioconvection number, porosity parameter, magnetic parameter, and Reynolds number, there is a reduction in flow characteristics.
2) The motion of fluid grows up with the augmenting values of the buoyancy parameter, which leads to an augmentation in the velocity profiles.
3) The rising values of Brownian motion and thermophoretic factors support the thermal flow and oppose the mass flow.
4) The growth in the radiation parameter and Reynolds number causes an augmentation in the temperature of the fluid.
5) With the augmenting values of the chemical reaction, the fluid molecular diffusivity reduces, due to which less mass diffuses, which causes a decline in the concentration of the fluid. On the other hand, with the augmenting values of the activation energy factor, the concentration profiles grow up.
6) For growth in Lewis and Prandtl numbers, there is a decline in the mass flow that results in a decay in the concentration profile.
7) The growth in the temperature ratio results in an augmentation in the temperature difference that leads to more thermal flow at free stream due to which the diffusivity of mass in the closed vicinity of the cylinder reduces and weakens the concentration profile.
8) An augmentation in the Peclet number leads to a decline in the diffusivity of motile microorganisms that declines the profile for microorganisms.

9) The statistical data for the enhancement in skin friction, Nusselt number, and motile microorganisms due to various parameters are shown in Chart 1, 2, and 3, respectively.

Data availability statement

The raw data supporting the conclusions of this article will be made available by the authors, without undue reservation.

Author contributions

AK modeled the problem. AK and ZI wrote the manuscript. AK and SE solved the modeled problem by the homotopy analysis method.

Acknowledgments

Conflict of interest

The authors declare that the research was conducted in the absence of any commercial or financial relationships that could be construed as a potential conflict of interest.

Publisher's note

All claims expressed in this article are solely those of the authors and do not necessarily represent those of their affiliated organizations, or those of the publisher, the editors, and the reviewers. Any product that may be evaluated in this article, or claim that may be made by its manufacturer, is not guaranteed or endorsed by the publisher.

References

1. Platt JR. Bioconvection patterns in cultures of free-swimming organisms. *Science* (1961) 133(3466):1766–7. doi:10.1126/science.133.3466.1766

2. Ahmad I, Aziz S, Ali N, Khan SU, Khan MI, Tlili I, et al. Thermally developed Cattaneo-Christov Maxwell nanofluid over bidirectional periodically accelerated surface with gyrotactic microorganisms and activation energy. *Alexandria Eng J* (2020) 59(6):4865–78. doi:10.1016/j.aej.2020.08.051

3. Sajid T, Tanveer S, Munsab M, Sabir Z. Impact of oxytactic microorganisms and variable species diffusivity on blood-gold Reiner–Philippoff nanofluid. *Appl Nanoscience* (2021) 11(1):321–33. doi:10.1007/s13204-020-01581-x

4. Waqas H, Hussain M, Alqarni MS, Eid MR, Muhammad T. Numerical simulation for magnetic dipole in bioconvection flow of Jeffrey nanofluid with swimming motile microorganisms. *Waves in Random and Complex Media* (2021) 1–18. doi:10.1080/17455030.2021.1948634

5. Shahzad F, Jamshed W, Sajid T, Shamshuddin MD, Safdar R, Salawu SO, et al. Electromagnetic control and dynamics of generalized burgers' nanoliquid flow containing motile microorganisms with Cattaneo–Christov relations: Galerkin finite element mechanism. *Appl Sci* (2022) 12(17):8636. doi:10.3390/app12178636

6. Safdar R, Gulzar I, Jawad M, Jamshed W, Shahzad F, Eid MR. Buoyancy force and Arrhenius energy impacts on Buongiorno electromagnetic nanofluid flow containing gyrotactic microorganism. *Proc Inst Mech Eng C: J Mech Eng Sci* (2022) 236:9459–71. doi:10.1177/09544062221095693

7. Abdelmalek Z, Khan SU, Waqas H, Riaz A, Khan IA, Tlili I. A mathematical model for bioconvection flow of Williamson nanofluid over a stretching cylinder featuring variable thermal conductivity, activation energy and second-order slip. *J Therm Anal Calorim* (2020) 144:205–17. doi:10.1007/s10973-020-09450-z

8. Hamid A, Khan MI, Kumar RN, Gowda RP, Prasannakumara BC. *Numerical study of bio-convection flow of magneto-cross nanofluid containing gyrotactic microorganisms with effective Prandtl number approach* (2021).

9. Rana BMJ, Arifuzzaman SM, Islam S, Reza-E-Rabbi S, Al-Mamun A, Mazumder M, et al. Swimming of microbes in blood flow of nano-bioconvective Wiliamson fluid. *Therm Sci Eng Prog* (2021) 25:101018. doi:10.1016/j.tsep.2021.101018

10. Chamkha AJ, Rashad AM, Al-Mudhaf HF. Heat and mass transfer from truncated cones with variable wall temperature and concentration in the presence of chemical reaction effects. *Int J Numer Method H* (2012) 22:357–76. doi:10.1108/09615531211208060

11. Mabood F, Nayak MK, Chamkha AJ. Heat transfer on the cross flow of micropolar fluids over a thin needle moving in a parallel stream influenced by binary chemical reaction and Arrhenius activation energy. *The Eur Phys J Plus* (2019) 134(9):427. doi:10.1140/epjp/i2019-12716-9

12. Sarada K, Gamaoun F, Abdulrahman A, Paramesh SO, Kumar R, Prasanna GD, et al. Impact of exponential form of internal heat generation on water-based ternary hybrid nanofluid flow by capitalizing non-Fourier heat flux model. *Case Stud Therm Eng* (2022) 38:102332. doi:10.1016/j.csite.2022.102332

13. Arrhenius S. Über die Dissociationswärme und den Einfluss der Temperatur auf den Dissociationsgrad der Elektrolyte. *Z für physikalische Chem* (1889) 4(1):96–116. doi:10.1515/zpch-1889-0108

14. Maleque K. Effects of exothermic/endothermic chemical reactions with Arrhenius activation energy on MHD free convection and mass transfer flow in presence of thermal radiation. *J Thermodynamics* (2013) 2013:1–11. doi:10.1155/2013/692516

15. Jayaprakash MC, Alsulami MD, Shanker B, Varun Kumar RS. Investigation of Arrhenius activation energy and convective heat transfer efficiency in radiative hybrid nanofluid flow. *Waves in Random and Complex Media* (2022) 1–13. doi:10.1080/17455030.2021.2022811

16. Sajid T, Ayub A, Shah SZH, Jamshed W, Eid MR, El Din ESMT, et al. Trace of chemical reactions accompanied with Arrhenius energy on ternary hybridity nanofluid past a wedge. *Symmetry* (2022) 14(9):1850. doi:10.3390/sym14091850

17. Choi SUS. Enhancing thermal conductivity of fluids with nanoparticles. In: DA Siginer HP Wang, editors. *Developments and applications of non-Newtonian flows, FED*. New York: ASME (1995). p. 99–105. vol. 231/MD-vol. 66.

18. Sajid T, Jamshed W, Shahzad F, Ullah I, Ibrahim RW, Eid MR, et al. Insightful into dynamics of magneto Reiner-Philippoff nanofluid flow induced by triple-diffusive convection with zero nanoparticle mass flux. *Ain Shams Eng J* (2022) 101946. doi:10.1016/j.asej.2022.101946

19. Sajid T, Jamshed W, Shahzad F, Akgül EK, Nisar KS, Eid MR. Impact of gold nanoparticles along with Maxwell velocity and Smoluchowski temperature slip boundary conditions on fluid flow: Sutterby model. *Chin J Phys* (2022) 77:1387–404. doi:10.1016/j.cjph.2021.11.011

20. Sajid T, Jamshed W, Safdar R, Hussain SM, Shahzad F, Bilal M, et al. Features and aspects of radioactive flow and slippage velocity on rotating two-phase Prandtl nanofluid with zero mass fluxing and convective constraints. *Int Commun Heat Mass Transfer* (2022) 136:106180. doi:10.1016/j.icheatmasstransfer.2022.106180

21. Saleem S, Animasaun IL, Yook SJ, Al-Mdallal QM, Shah NA, Faisal M. Insight into the motion of water conveying three kinds of nanoparticles shapes on a horizontal surface: Significance of thermo-migration and Brownian motion. *Surf Inter* (2022) 30:101854. doi:10.1016/j.surfin.2022.101854

22. Cao W, Animasaun IL, Yook SJ, Oladipupo VA, Ji X. Simulation of the dynamics of colloidal mixture of water with various nanoparticles at different levels of partial slip: Ternary-hybrid nanofluid. *Int Commun Heat Mass Transfer* (2022) 135:106069. doi:10.1016/j.icheatmasstransfer.2022.106069

23. Animasaun IL, Yook SJ, Muhammad T, Mathew A. Dynamics of ternary-hybrid nanofluid subject to magnetic flux density and heat source or sink on a convectively heated surface. *Surf Inter* (2022) 28:101654. doi:10.1016/j.surfin.2021.101654

24. Xiu W, Animasaun IL, Al-Mdallal QM, Alzahrani AK, Muhammad T. Dynamics of ternary-hybrid nanofluids due to dual stretching on wedge surfaces when volume of nanoparticles is small and large: Forced convection of water at different temperatures. *Int Commun Heat Mass Transfer* (2022) 137:106241. doi:10.1016/j.icheatmasstransfer.2022.106241

25. Kumar RN, Gowda RP, Abusorrah AM, Mahrous YM, Abu-Hamdeh NH, Issakhov A, et al. Impact of magnetic dipole on ferromagnetic hybrid nanofluid flow over a stretching cylinder. *Physica Scripta* (2021) 96(4):045215. doi:10.1088/1402-4896/abe324

26. Naveen Kumar R, Punith Gowda RJ, Prasanna GD, Prasannakumara BC, Nisar KS, Jamshed W. Comprehensive study of thermophoretic diffusion deposition velocity effect on heat and mass transfer of ferromagnetic fluid flow along a stretching cylinder. *Proc Inst Mech Eng E: J Process Mech Eng* (2021) 235(5):1479–89. doi:10.1177/09544089211005291

27. Varun Kumar RS, Punith Gowda RJ, Naveen Kumar R, Radhika M, Prasannakumara BC. Two-phase flow of dusty fluid with suspended hybrid nanoparticles over a stretching cylinder with modified Fourier heat flux. *SN Appl Sci* (2021) 3(3):384–9. doi:10.1007/s42452-021-04364-3

28. Benaziza N, Nacereddine MK, Kezzar M, Sari MR, Khounfais K, Eid MR. Entropy generation in magneto-nanofluid flow between two coaxial cylinders by using a new i-adm technique. *Comput Therm Sci Int J* (2021) 13(6):33–51. doi:10.1615/computthermalscien.2021038214

29. Eid MR, Al-Hossainy AF, Zoromba MS. FEM for blood-based SWCNTs flow through a circular cylinder in a porous medium with electromagnetic radiation. *Commun Theor Phys* (2019) 71(12):1425. doi:10.1088/0253-6102/71/12/1425

30. Jamshed W, Eid MR, Hussain SM, Abderrahmane A, Safdar R, Younis O, et al. Physical specifications of MHD mixed convective of Ostwald-de Waele nanofluids in a vented-cavity with inner elliptic cylinder. *Int Commun Heat Mass Transfer* (2022) 134:106038. doi:10.1016/j.icheatmasstransfer.2022.106038

31. Punith Gowda RJ, Naveen Kumar R, Prasannakumara BC. Two-phase Darcy-Forchheimer flow of dusty hybrid nanofluid with viscous dissipation over a cylinder. *Int J Appl Comput Math* (2021) 7(3):95–18. doi:10.1007/s40819-021-01033-2

32. Khan M, Irfan M, Khan WA, Sajid M. Consequence of convective conditions for flow of Oldroyd-B nanofluid by a stretching cylinder. *J Braz Soc Mech Sci Eng* (2019) 41(3):116. doi:10.1007/s40430-019-1604-3

33. Forchheimer P. Wasserbewegung durch boden. *Z Ver Deutsch, Ing* (1901) 45:1782–8.

34. Muskat M. The flow of homogeneous fluids through porous media. In: JW Edwards, editor. *Ann arbor, mich*, 191 (1946).

35. Pandey AK, Kumar M. Natural convection and thermal radiation influence on nanofluid flow over a stretching cylinder in a porous medium with viscous dissipation. *Alexandria Eng J* (2017) 56(1):55–62. doi:10.1016/j.aej.2016.08.035

36. Benos LT, Polychronopoulos ND, Mahabaleshwar US, Lorenzini G, Sarris IE. Thermal and flow investigation of MHD natural convection in a nanofluid-saturated porous enclosure: An asymptotic analysis. *J Therm Anal Calorim* (2021) 143(1):751–65. doi:10.1007/s10973-019-09165-w

37. Redouane F, Jamshed W, Devi S, Amine BM, Safdar R, Al-Farhany K, et al. Influence of entropy on Brinkman-Forchheimer model of MHD hybrid nanofluid flowing in enclosure containing rotating cylinder and undulating porous stratum. *Scientific Rep* (2021) 11(1):24316–26. doi:10.1038/s41598-021-03477-4

38. Anwar Bég O, Mahabaleshwar US, Rashidi MM, Rahimzadeh N, Curiel-Sosa JL, Sarris I, et al. Homotopy analysis of magnetohydrodynamic convection flow in manufacture of a viscoelastic fabric for space applications. *Int J Appl Math Mech* (2014) 10:9–49.

39. Liao SJ. An optimal homotopyanalysis approach for strongly nonlinear differential equations. *Commun Nonlinear Sci Numer Simul* (2010) 15:2003–16. doi:10.1016/j.cnsns.2009.09.002

40. Imtiaz M, Hayat T, Alsaedi A. Mixed convection flow of Casson nanofluid over a stretching cylinder with convective boundary conditions. *Adv Powder Tech* (2016) 27(5):2245–56. doi:10.1016/j.apt.2016.08.011

41. White FM. *Viscous fluid flow 2nd edn*. New York: McGraw-Hill (1991).

42. Ahmed A, Khan M, Ahmed J. Thermal analysis in swirl motion of Maxwell nanofluid over a rotating circular cylinder. *Appl Math Mech* (2020) 41(9):1417–30. doi:10.1007/s10483-020-2643-7

43. Hayat T, Khan MI, Waqas M, Alsaedi A. Newtonian heating effect in nanofluid flow by a permeable cylinder. *Results Phys* (2017) 7:256–62. doi:10.1016/j.rinp.2016.11.047

44. Waqas H, Imran M, Bhatti MM. Influence of bioconvection on Maxwell nanofluid flow with the swimming of motile microorganisms over a vertical rotating cylinder. *Chin J Phys* (2020) 68:558–77. doi:10.1016/j.cjph.2020.10.014

45. Islam S, Khan A, Kumam P, Alrabaiah H, Shah Z, Khan W, et al. Radiative mixed convection flow of Maxwell nanofluid over a stretching cylinder with joule heating and heat source/sink effects. *Scientific Rep* (2020) 10(1):17823–18. doi:10.1038/s41598-020-74393-2

46. Khan A, Saeed A, Gul T, Mukhtar S, Ali I, Jawad M. Radiative swirl motion of hydromagnetic Casson nanofluid flow over rotary cylinder using Joule dissipation impact. *Physica Scripta* (2021) 96(4):045206. doi:10.1088/1402-4896/abdf83

Nomenclature

u, w axial, radial factors of velocity (m/s)

B_0 constant magnetic field (kg/s^2A)

T fluid temperature (K)

T_w wall temperature (K)

T_∞ free steam temperature (K)

C concentration of the fluid

C_w concentration of the wall

C_∞ free stream concentration

D_B coefficient of Brownian diffusion (m^2/s)

D_T coefficient of thermophoretic diffusion (m^2/s)

Re Reynolds number

M magnetic factor

N_b Brownian factor

N_t thermophoresis factor

R_d radiation factor

E dimensionless activation energy factor

Pr Prandtl number

Le Lewis number

L_b bioconvection Lewis number

Pe Peclet number

Nu Nusselt number

Sh Sherwood number

Nn microorganism density number

R_1 radius of the cylinder

k thermal conductivity $(W/k.m)$

Greek symbols

τ heat capacity ratio

θ dimensionless temperature

φ dimensionless concentration

ρ density of the fluid (kg/m^3)

α thermal diffusivity (m/s)

η coordinate of transformation

υ kinematic viscosity (m^2/s)

ε_1 thermal Biot number

μ dynamic viscosity (kg/m^2s)

Abbreviations

MHD, magnetohydrodynamic;

HAM, homotopy analysis method;

ODEs, ordinary differential equations.